

IRAS 04210+0400 : Modeling the optical spectra from flaring large scale jets

W. Steffen,¹ A.J. Holloway,¹ A. Pedlar²

¹*Department of Astronomy, University of Manchester, Schuster Laboratory, Oxford Road, Manchester M13 9PL, UK*

²*Nuffield Radio Astronomy Laboratories, University of Manchester, Jodrell Bank, Macclesfield, Cheshire SK11 9DL, UK*

Empty

ABSTRACT

The emission-lines in the active galaxy IRAS 0421+0400 show a dramatic ($\sim 900 \text{ km s}^{-1}$) increase in the velocity spread at the position of radio hot-spots which are located at the beginning of extended radio lobes. We study a simple geometric model of an opening outflow which reproduces the structure found in the long-slit emission-line spectrum of the hot-spot regions. The predicted bifurcations in the optical image structure of these regions is confirmed by deep [OIII]-5007Å line-imaging. We propose that this phenomenon is the result of a jet emerging from the galaxy through the boundary between the interstellar and intergalactic medium. A similar model has previously been suggested as an explanation for wide angle tail radio sources (WAT's). If our model proves to be correct in more detailed future observations, then IRAS 0421+0400 provides the unique possibility to study the flaring jet phenomenon at optical wavelengths.

Key words: galaxies: active - galaxies: individual: IRAS 04210+0400 - galaxies: jets - galaxies: kinematics and dynamics - galaxies: Seyfert

1 INTRODUCTION

Jets in FRI radio galaxies can flare very abruptly and show very large opening angles up to 90° in diffuse lobes or tails (O'Donoghue et al. 1993). These structures often bend near the flaring point. Norman et al. (1988) and Loken et al. (1995) have modelled this phenomenon in wide angle tail radio galaxies (WAT) in terms of a supersonic jet passing through a shock in the ambient gas where the jet flow becomes subsonic. The jet is then disrupted and entrains external gas, which becomes turbulent with the formation of large and small scale eddies. Such a shock in the ambient medium could be due to a supersonic galactic wind moving into the surrounding intergalactic medium.

In order to obtain direct kinematic information, Owen et al. (1990) conducted a search for optical line emission from the flaring regions in WAT sources but found no significant emission from the 5 objects they studied. In Holloway et al. (1996, Paper I) we first proposed that a phenomenon similar to the WATs could apply to IRAS 04210+0400 for which optical information is available in the flaring region (Beichman et al. 1985; Hill et al. 1988; Holloway et al. 1996). If our interpretation is correct, then IRAS 0421+0400 is an important test object allowing us to study such a transition region in the optical regime, thereby providing important kinematic information from spatially resolved spectra.

The active galaxy IRAS 0421+0400 was discovered on

scans of the Infrared Astronomical Satellite (IRAS) by (Soifer et al. 1984). Beichman et al. (1985) identified the IRAS source with a spiral galaxy at a red-shift of $z=0.046$. Their spectroscopic work revealed a Seyfert-2-type emission-line nucleus of the 16.3 magnitude (R-band) object. First observations with the Very Large Array (VLA) showed an unusual radio structure, consisting mainly of large symmetrically bent lobes ($\sim 25 \text{ kpc}$), which seemed to extend the spiral structure beyond the optically detected image (Beichman et al. 1985). Hill et al. (1988) reported the discovery of a central double radio source ($\sim 1''$ separation) and that the lobes start at hot-spots which are coincident with anomalous spectral features (Steffen et al. 1996a). They found that at the position of the hot-spot the spectral lines consisted mainly of an asymmetric narrow ($\text{fwhm} = 160 \text{ km s}^{-1}$) and a broad ($\text{fwhm} = 730 \text{ km s}^{-1}$) component. They argued that the extended spiral features found in this galaxy are the photoionized remnants of earlier radio jet activity. Steffen et al. (1996b) examined this model in some detailed and concluded that it was not consistent with the observations and suggested an alternative model based on the bending of the jets by the interaction with the rotating interstellar medium.

In Paper I we identified broad red and blue shifted velocity components (north and south of the continuum peak, respectively) with similar spatial separation as the central double radio source. We spatially resolved the broad spectral features near the radio hot-spots and presented first results

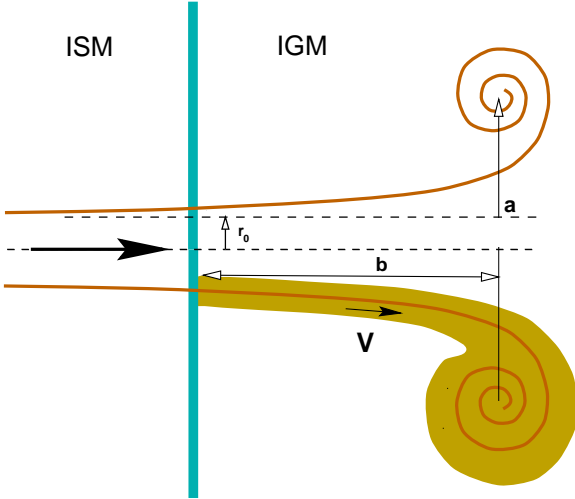


Figure 1. In this line drawing the geometric model parameters of the flow are illustrated. They are the initial radius of the circular cross section r_0 , the distance b of the eddy from the transition region, where the emission is assumed to start, and the distance $r_0 + a$ from the axis.

from a model which explains the spectra as a consequence of an opening cone starting at the radio hot-spots. As pointed out in Paper I, the origin of these structures seems to be related to the flaring of the radio structure into extended lobes.

Hubble Space Telescope (HST) observations of IRAS04210+0400 presented by Capetti et al. (1996) spatially resolve the central region into a complex structure with discrete emission-line clouds. There are three particularly bright knots, confirming the triple structure deduced in Paper I from spectroscopic observations. Capetti et al. (1996) also find filamentary high ionization line emission (coincident with the previously known spiral features) which bifurcates close to the southern radio hot-spot. This strongly supports the model proposed in Paper I involving a flaring jet at this position.

In the present paper, we give a more detailed account of the model first proposed in Paper I. In Section 2 we introduce the model, discussing the dependence of the spectral line-shape on the orientation of the outflow with respect to the observer and the direction of the spectrometer slit. In Section 3 we compare our model with the observations, which we summarize at the beginning. In the same section a new deep emission-line image is presented. We discuss and summarize our results in Sections 4 and 5, respectively.

2 THE MODEL

In this section we describe a simple model which is intended to provide some insight into the existent gross emissivity and flow distribution in the emission-line gas associated with the extended radio emission in IRAS04210+0400. We model the long-slit spectra using a simple parameterized description of the emissivity and the velocity field of the ionized gas flow. In our model we regard the extended emission-line source around the radio hot-spots as a collimated outflow

which flares when passing through the boundary between the ISM and the IGM (see Figure 1).

First we give the details about the parameterization used in this model. We then discuss the general properties of the predicted images and spectra as a function of orientation in space. After discussing the observational constraints, we present a simple axisymmetric and an improved non-axisymmetric solution which match the observations in some details.

2.1 Parameterization of the model

Hydrodynamic simulations (Loken et al. 1995) suggest that large-scale eddies often develop in the flaring regions of jets crossing an external shock and that they can approximately be described by a circular or spiraling sheet with flow velocities comparable to the boundaries of the flaring jet region. For simplicity we parameterize this flow as a hyperbolic spiral given by

$$z'(s) = -\frac{a}{s} \cos(s) + \frac{a}{s_0} \cos(s_0) \quad (1)$$

$$r(s) = \{r_0 + a[1 - \sin(s)/s]\}/\epsilon \quad (2)$$

$$\epsilon = [1 - e \cos(\phi)]/(1 - e). \quad (3)$$

Here (z', r, ϕ) are cylindrical coordinates, and s is a normalized position parameter along the spiral (with $s_0 = -b/a + \sqrt{2 + (b/a)^2}$). The parameter r_0 is the initial radial distance from the axis, while ϵ allows for an elliptic cross section of eccentricity e as a simple approximation to non-axisymmetry. The distance between the centre of the eddy and the axis is given by $r_0 + a$. The parameters a and b are as indicated in Figure 1. The orientation of the outflow in space is determined by the Euler angles (Θ, Φ, Ψ) with the conventions given in Goldstein (1980).

The calculations are performed on a regular 3-dimensional cartesian grid (x, y, z) , with the z -axis along the line of sight. The z -axis of the cartesian coordinate system coincides with the z' -axis of the cylindrical system used for the representation of the outflow in Equations 2 & 3 when the Euler-angle $\Theta = 0$. Typical array sizes of the calculations presented here are 80-100 pixels (≈ 10 pixels per arcsec) along a side of the cubic domain. Since we are considering mainly forbidden lines ([OIII]-5007Å & [NII] 6584-Å), the emission is assumed to be optically thin. The image intensity is therefore calculated by adding the emissivity in each pixel along the line of sight.

2.2 Dependence of the spectrum on orientation

The long-slit line profile is most dependent on the orientation of the outflow with respect to the observer's line of sight and the orientation of the spectrometer slit. This is true for full slit-coverage of the outflow. If the slit does not cover the whole structure, the resulting spectrum is also strongly dependent on the slit position. This dependence is discussed in more detail in Section 3.5. The detailed shape of the outflow and the change in emissivity as a function of distance from the starting point (as, for instance, a slow decrease in emissivity compared to a constant emissivity) only influence the details of the simulated spectrum and not the gross

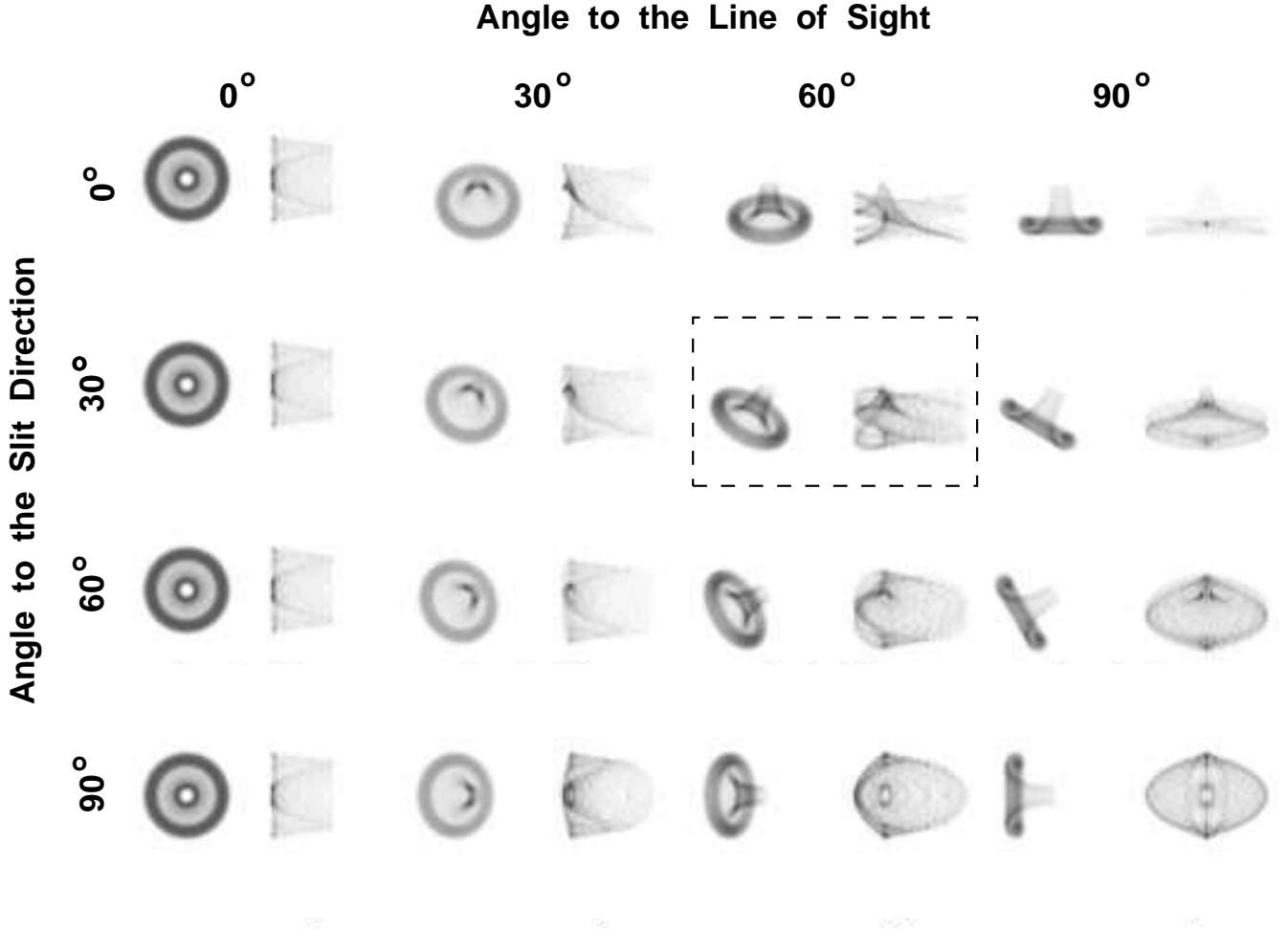


Figure 2. A series of simulations of an opening outflow is shown varying the orientation of the axis with respect to the line of sight (left to right) and the slit orientation. The slit runs from top to bottom and covers the whole emission. Represented are pairs of images (left) and long-slit spectra (right). The simulation marked with a dashed box is shown in more detail in the next figure. In this series it is the closest match to the observations at the southern hot-spot region in IRAS 0421+0400, and it was used as a starting point for more detailed simulations which are compared to the observations below.

features. The optical emission is rather sensitive to temperature and density of the flow, and these change considerably where the outflow turns back and becomes turbulent (Loken et al. 1995). It can therefore be expected that optical emission drops drastically near this point, rendering the eddies very faint or undetectable. Therefore, we assume a constant emissivity and velocity along the flow line and a Gaussian transverse emissivity distribution of $\text{FWHM} = 0.5r_0$, with a cut-off at position $s = s_f$ along the spiral (which we expect to be near the turning point).

In Figure 2 we show a series of results for axisymmetric outflows varying the angle between the axis and the line of sight (left to right) and orientation with respect to the direction of the spectrometer slit (which covers the whole structure). A nonlinear grey-scale is used to emphasize the background emission in the spectra which arises mostly from the eddies. The outflows shown here are directed towards the observer. The emission is therefore mainly blue-shifted. Since we are considering only optically thin emission, corresponding orientations away from the observer produce symmetrically red-shifted spectra and are omitted. For most orienta-

tions the opening section of the outflow produces a bright, asymmetric, and opening feature in the spectrum which is often ‘ Λ ’-shaped (or ‘V’-shaped, if the outflow is oriented in opposite direction). The eddies generally result in a diffuse distribution around the emission arising from the outflow. The simulation marked with a dashed box in the mosaic (Figure 2) is shown in detail in Figure 4 with the outflowing region emphasized in the image and the spectrum. It shows the back-flow can produce loop-like structures.

In Figure 3 we display the integrated spectra corresponding to the simulations in the mosaic. Note that the spectra in each column of Figure 2 have the same integrated spectra and need to be spatially resolved to be distinguishable from each other. The integrated spectra consist of blue-shifted peaks with broad wings mainly from the eddies.

3 OBSERVATIONS

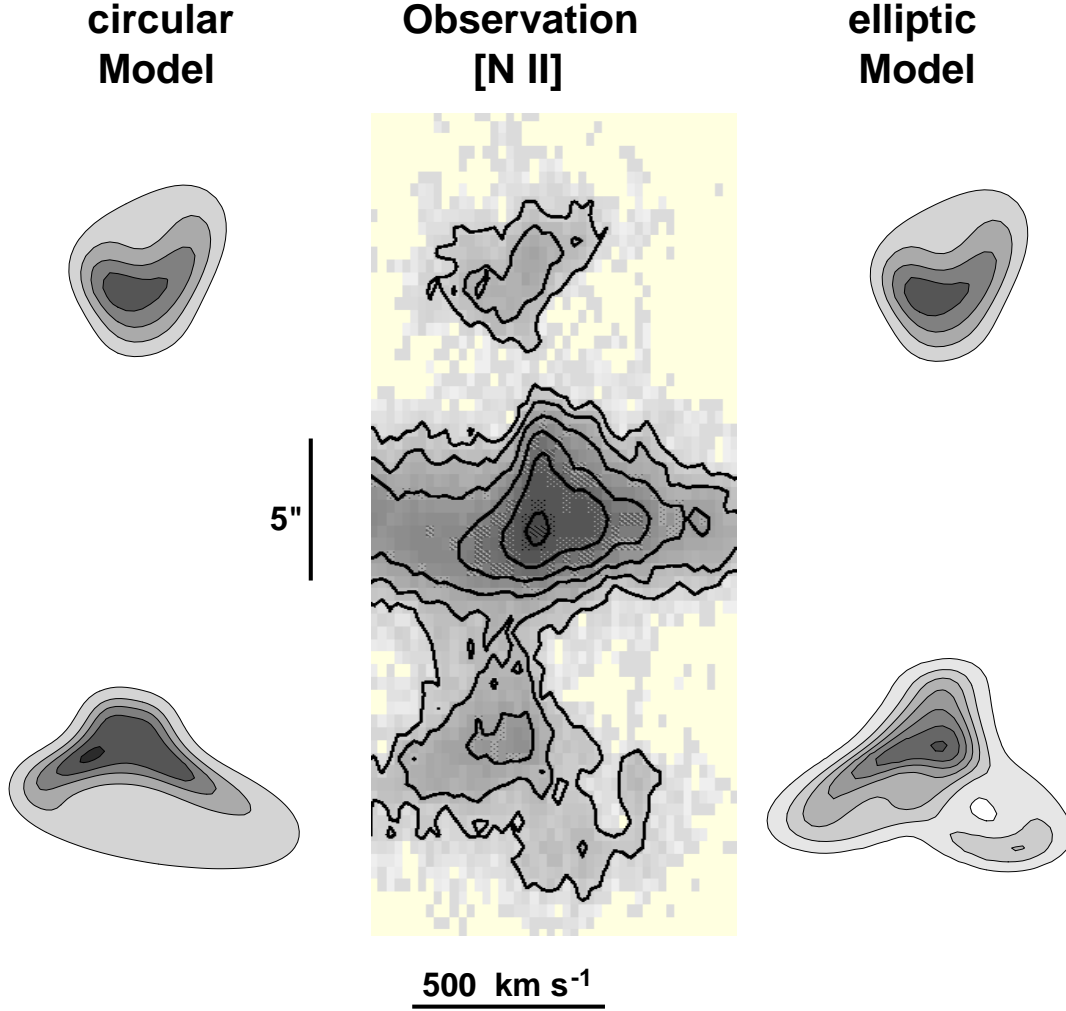


Figure 5. The observed [NII] 6584-Å long-slit spectrum (middle) is compared to our model. On the left the model with the fully circular cross section is represented. On the right of the observations, the results for model variant with an elliptic cross section in the southern outflow are displayed. Observe the flaring of the spectra at approx. 5 arcsec to the north and south of the centre.

Table 1. The geometric parameters and the velocity v of the simulations, which we compare with the observations are given. The first two rows are axisymmetric simulations of the northern (N) and southern (S). (Θ, Φ, Ψ) are the Euler angles giving the orientation in space with the conventions of Goldstein (1980). Herein Θ is to the angle with respect to the line of sight and Ψ corresponds the angle with respect to the slit orientation. The azimuthal orientation of the outflow on the axis is given by Φ . The point at which the emission ceases along the outflow is s_f .

e		v	Θ	Φ	Ψ	b/a	s_f
0	(N)	350	100°	—	35°	0.45	1.7
0	(S)	500	−105°	—	30°	0.8	2.5
0.7	(S)	500	−75°	−35°	35°	0.5	3.2

3.1 Long-slit spectra

The long-slit observations to which we apply our model where presented in Paper I, therefore suffice to summarize the main properties which are important for our model. The

basic structure can be appreciated best in the [NII] 6584-Å line, which we reproduce in Figure 5. The northern hot-spot at around 5'' separation from the centre shows a ‘V’-shaped structure, where the red-shifted arm is stronger and more extended.

The southern hot-spot shows a very similar, ‘Λ’-structure, which is better defined: most of the emission spreads into a blue wing. At a lower brightness level, emission is seen in a red wing. The observation is suggestive of two or more discrete components or possibly a ring-like structure in the velocity-space map. A considerably different picture is seen in the [OIII]-5007Å line (reproduced in Figure 6). Here the ‘Λ’-shape is not obvious. Instead, all or most emission seems to be in one of the red-shifted components also seen in the [NII] 6584-Å line.

As mentioned in Paper I, there are three simple possible kinematic interpretations of such ‘Λ’-shaped structures in the velocity map. First, they may arise from real acceleration of the gas. Alternatively, the gas might have a certain high velocity when the line emission starts and only the direction of the velocity vector changes along its trajectory. Naturally,

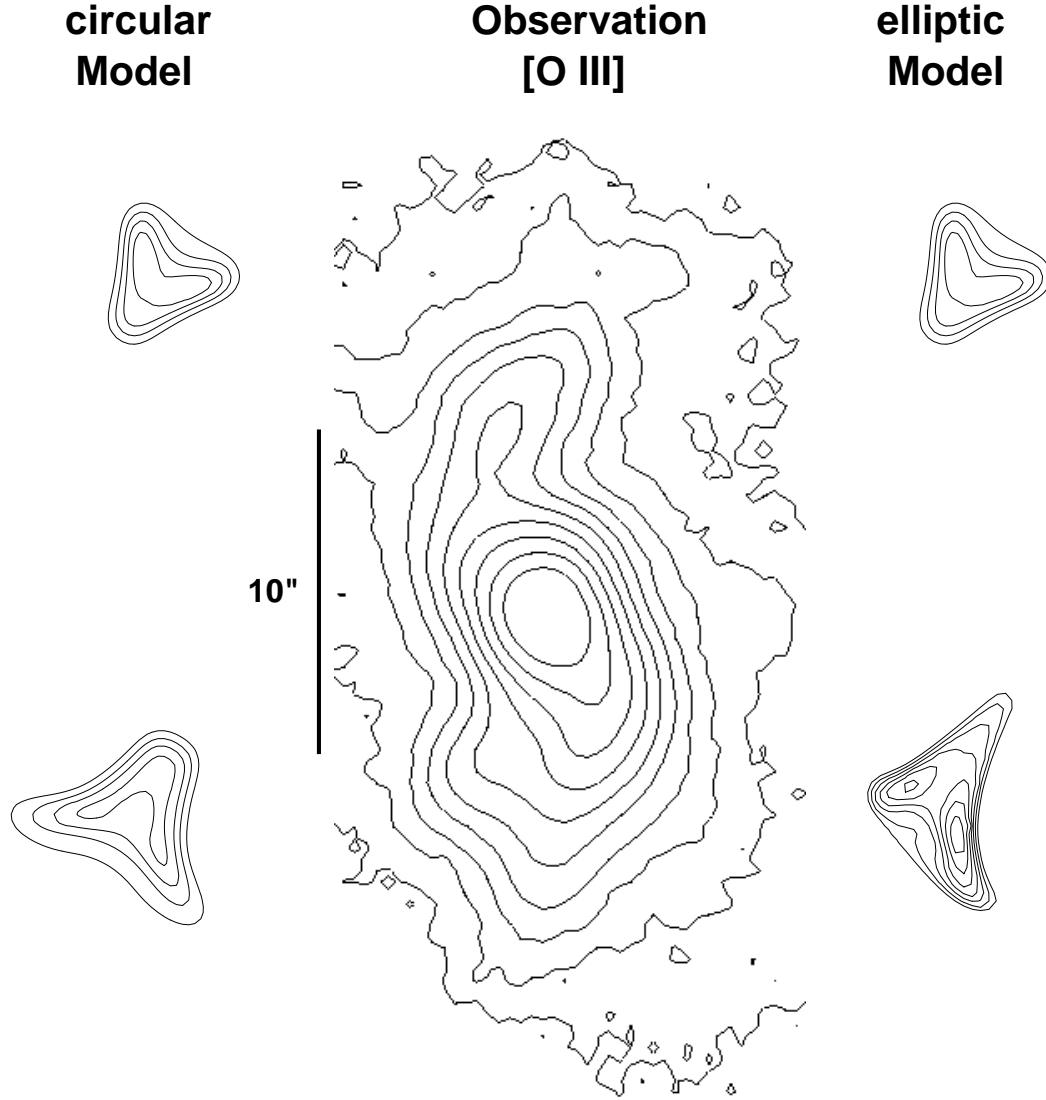


Figure 7. The middle section shows the observed [O III]-5007Å emission-line image of IRAS 04210+0400 . Note the bifurcations to the north and south of the centre, which we identify with the opening outflows. The predicted model images of the flaring regions in the case of an axisymmetric outflow are shown on the left side of the observations. On right, the simulation where the southern hot-spot region has an elliptic cross section is represented. Contour levels of the observation are 0.5, 1, 1.5, 3, 6, 10, 15, 25, 40, 60 % of the peak brightness. For clarity, the contours of the simulated images have equally spaced contours.

the third possibility is a combination of both effects. The bifurcations found in the new optical line images presented in the next section provide new evidence for our model of an opening out-flow, in which the flaring of the spectra in the hot-spots is dominated by geometric effects (i.e. the flow direction changes along the streamlines).

3.2 New emission-line imaging

In Figure 9 (Plate 1) we present a new [O III] 5007-Å emission-line image of IRAS 04210+0400 . It is a composite of three images of 30 minutes exposure time each, obtained at the Anglo-Australian Telescope (AAT) with an [O III] 5007-Å filter (bandwidth 70Å). We show two versions of the same data. At the top of Figure 9 the galaxy is shown including its near environment with the grey-scale chosen such that the fainter extended emission is emphasized. In

the bottom picture the bright central spiral structure is emphasized. The seeing varied from 1 to 2 arcsec between the individual exposures. The image confirms the central structure observed previously by Beichman et al. (1985). It shows the bifurcation of the ‘spiral arm’ in the south, which is also present in the HST-image obtained by Capetti et al. (1996). However, our deep ground-based image clearly reveals a faint bifurcation of the extended emission-line spiral arm beyond the northern hot-spot region. This observation strongly supports our interpretation of the flaring of the emission-line width in these regions as an opening out-flow of emission-line gas. This northern ‘V’ is much fainter than the strong bifurcated southern ‘arm’.

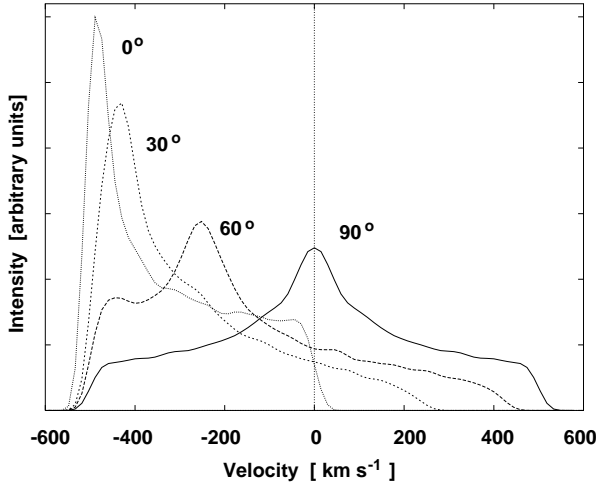


Figure 3. Integrated spectra are plotted which correspond to the long-slit spectra from the previous figure. Each of the four spectra represents all the long-slit spectra for a particular angle to the line of sight. The four integrated spectra are distinguished by the angle to the direction with respect to the slit, which is given beside the curves.

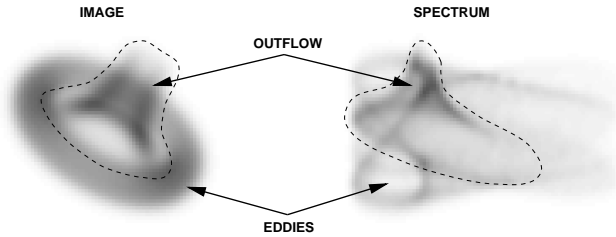


Figure 4. The simulation marked with a dashed line in the previous figure is shown in more detail. The out-flowing material, roughly marked with a dashed line in the image simulation (left), basically produces the marked region in the long-slit spectrum (right). Everything outside this region (and some background contribution to the inside region) is originated in the back-flow and eddy.

3.3 Constraints

Before we show the results of detailed models of the observations, we summarize the constraints which can be used as an input for the modeling process. From the new [OIII]-5007Å image, the projected direction (angle Θ) to the axis of the out-flow can be estimated from the orientation of the bifurcations. The result is consistent with the orientation of the radio lobes. We find that the approximate position angle of the bifurcations in the north is -35° and the south is 140° . Other constraints are the spatial extension and radial velocity width of the emission in the hot-spot regions, the asymmetry of the emission in the spectra, and the position of the maximum in the spectra, but which are more difficult to quantify.

The large parameter space has been explored by performing large numbers of intermediate resolution simulations (≈ 50 pixels along each axis) varying 2 parameters at a time. The parameter grid was chosen fine enough to ensure that only small changes were found between individual frames. The resulting series of images and spectra were

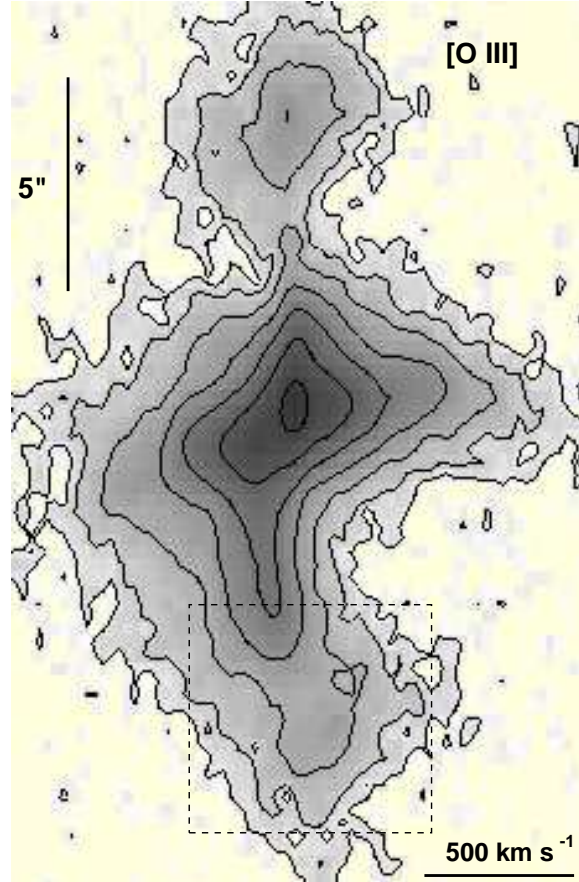


Figure 6. The long-slit profile of the [OIII]-5007Å line (from Paper I). The dashed box marks the southern hot-spot region.

inspected, and promising parameter sets were selected and refined. Although a few sets of parameters have been found which reproduce the observations partially, the solutions discussed in the following section give by far the best overall match between the simulation and the observations.

For direct comparison, the simulated images and spectra have been convolved with Gaussian point spread functions with FWHM similar to the resolutions of the observations (with 100 velocity channels).

3.4 Comparison between model and observations

In Figures 5 and 7 we compare the observed long-slit spectrum of the [NII] 6584-Å line and our new [OIII]-5007Å line-image, respectively, with our model. The simulation shown on the left is an axisymmetric calculation for both, the northern and the southern hot-spot region. The important parameters are given in rows 1 & 2 of Table 1. Note that the flaring and the rough brightness distribution in the spectrum are reproduced. However, one does also note that the red wing in the southern hot-spot is of similar strength as the blue wing. Also, the maximum emission is within the blue wing. These are general properties the axisymmetric simulations which fulfill the geometric constraints given in Section 3.3. They are in conflict with the observation.

These problems are solved in the simulation on the right side of Figures 5 & 7. Here the northern model is the same

as before, but an elliptic cross section according to Equation 3 was used with an eccentricity of $e = 0.7$. Similarly, the radial velocity component is now $v_{r(\phi)} = v_{r0}\epsilon(\phi)$. Note that the velocity is still constant along each flow line. In this variant of the model, the low brightness red-shifted section of the spectrum (with the shape of a loop) is produced close to the cut-off of the emissivity at s_f . Here the cut-off occurs where the out-flow starts to flow back, while in the axisymmetric case the emission cuts off before any back-flow or eddies develop. Note that extending the emission as far as in the elliptic case does not improve the result, but becomes completely inconsistent with the observation. The loop in the elliptic simulation is similar to the loop in Figure 4, only that the red-shifted emission is now blue-shifted and vice-versa (since it is pointing away from the observers instead of facing it).

Another improvement of the elliptic model over the axisymmetric case is seen from Table 1. In the axisymmetric simulation, the northern and the southern out-flow necessarily have to be pointing towards the observer, i.e. they are not co-linear (the angle between their axes is $\sim 155^\circ$). In contrast, in the non-axisymmetric simulation the axes form an angle of $\sim 175^\circ$, which is consistent with the projected symmetry suggested by the radio lobes.

3.5 Slit coverage and the [OIII]-5007Å line

In this section we consider the effect of slit coverage of the out-flow on the appearance of the spectrum. The simulations in the previous section assumed full coverage of the out-flow. We note however that the size of the slit in the observations was $1''$ and the images of the out-flows exceed this size in east-west direction. Another motivation for investigating reduced slit coverage was a significant qualitative difference between the southern hot-spot region in the [OIII]-5007Å line and the H α + [NII] complex. We suspect that this could be due to insufficient slit coverage. As can be seen in comparing Figures 5 and 6, the southern [OIII]-5007Å emission does not show the bright blue and red-shifted wings present in the H α + [NII] and the [SII] lines at $\sim 5''$ from the galaxy centre. A rather discrete red-shifted component is present at $\sim 7''$ core distance (see Figure 6).

We consider two possible explanations for this difference. The first of these concerns the uncertainty in the slit coverage of the relevant structures. We note that the H α + [NII] and [SII] (not all shown here) results are from a single observations, while the [OIII]-5007Å spectrum was obtained on another day and different seeing conditions. The second possibility is an intrinsic difference in the distribution, possibly caused by the different expansion velocities on a non-axisymmetric opening cone, which could result in different emission properties.

We performed a set of simulations involving a slit which only partially covers the image structures and step it from east to west. We used the non-axisymmetric simulation which compares best with the observations (Figure 5). In Figure 8 the area covered by the slit is marked by a box and the brightness is enhanced by a factor of 3 compared to the uncovered portion in the image. As expected the observed spectrum depends on the slit coverage. However, we also notice that, with the slit covering the central section of the out-flow, the upper panels contain all the essential spec-

tral features of the observed H α + [NII] lines as shown in the simulation with full coverage in Figure 5. This justifies the reduction of the number of free parameters by choosing full coverage in the simulation of observations with adequate slit positioning.

We also find that inadequate slit coverage could be the reason for the observed difference between the [OIII]-5007Å line and the H α + [NII] complex. The simulation on the lower right, with the slit covering only small image sections, compares well with the [OIII]-5007Å spectrum. The position of the [OIII]-5007Å feature is reproduced in position and spectral shift. From these considerations we conclude, that the observed difference between the observed [OIII]-5007Å and the corresponding H α + [NII] emission can be explained by an off-set in the positioning of the slit. It probably adequately covers the northern hot-spot region, but only partially intersects the southern counterpart. The shift of the slit position corresponds to $\sim 1.5''$ and is within the uncertainty of $\sim 2''$ from the positioning of the spectrometer slit during the observations.

This result provides the simplest explanation of the difference. However, as discussed in Section 4, it cannot rule out an intrinsic origin of the difference. Note that in the framework of our model, the [OIII]-5007Å component arises close to the end of the opening cone. A final decision can only be made with further observations with full spectroscopic coverage and detailed physical modeling of the suggested boundary layer between the jet material and the external medium.

4 DISCUSSION

We considered the kinematics in the extended emission-line region of the active galaxy IRAS 04210+0400. The distribution and kinematics of the emission-line gas seems to be strongly linked to the expansion of extended radio lobes. We have presented a simple model which describes the emission as an opening cone with possible eddies. We calculated model spectra of such out-flows varying the orientation with respect to the observer's line of sight and the orientation of the spectrometer slit (the most important parameters determining the shape of the long-slit spectra). We find that the main features of the observed long-slit spectra of the extended emission can be explained in terms of two axisymmetric out-flows which open very rapidly (over ~ 1 kpc at a projected distance of ~ 4.5 kpc).

Both, image and spectrum of the northern hot-spot region are well described by the axisymmetric model. However, the axisymmetric case is only of limited use for the southern hot-spot region which shows more detailed structure. A significant deviation of the axisymmetric model spectra from the observations of the southern hot-spot region is eliminated allowing for considerable non-axisymmetry of the out-flow. Even the simplest possible case, an elliptic cross section provides a better match to the observations than the axisymmetric model. Moreover, the predicted image of the elliptic simulation (Figure 7, right) is in better agreement with our observations and the high resolution HST-image presented by Capetti et al. (1996).

From our considerations of the difference between the [OIII]-5007Å and the H α + [NII] spectra of the southern hot-

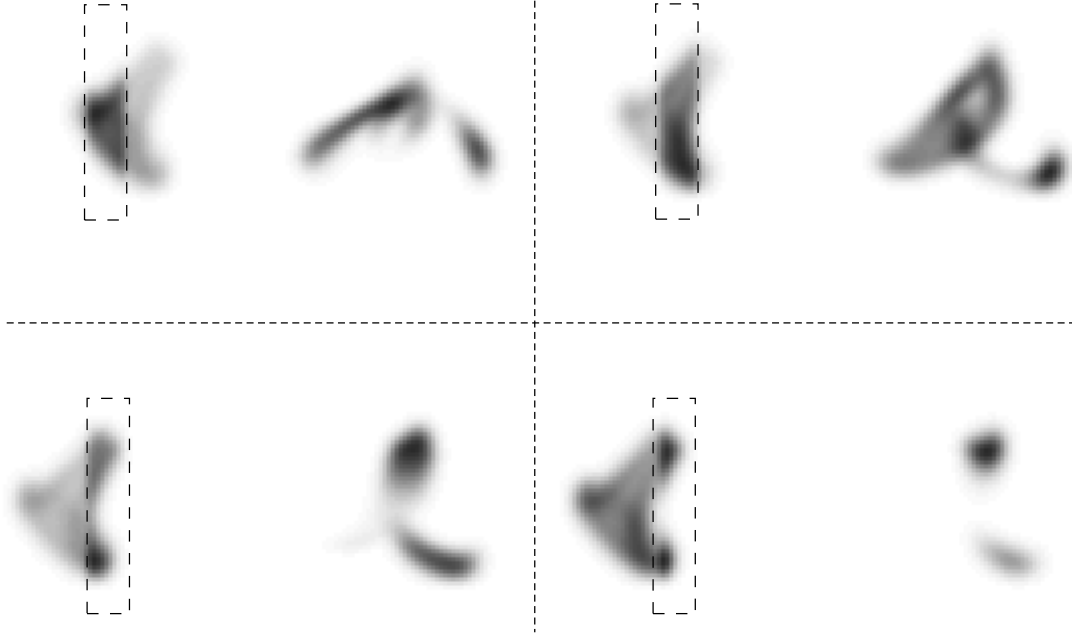


Figure 8. The southern out-flow with elliptic cross section is shown for different slit coverages. As in the previous Figures, the pairs of image (left) and long-slit spectrum (right) are shown. The section included in the spectrum is marked by a dashed box and with the intensity enhanced by a factor of three in the images.

spot region, we find that these could possibly be accounted for by insufficient slit coverage during the $[\text{OIII}]\text{-}5007\text{\AA}$ observation. Therefore, re-observation of the $[\text{OIII}]\text{-}5007\text{\AA}$ line with adequate coverage and sensitivity is desirable. If the difference is confirmed to be intrinsic, it could provide important information to test a more physical model based on the geometric approach of this paper.

We suggest that the most plausible process producing the morphology and the flow pattern represented by our model is a turbulent mixing layer similar to one described by Cantó & Raga (1991) which could develop rapidly after the jet crossed a shocked boundary between the interstellar and the intergalactic medium. However, in contrast to the conditions in their model, which was applied to a supersonic stellar jet, in our case we would have a hot internally subsonic flow, which heavily entrains external gas. This gas is heated and ionized. The temperature will rise from the edge towards the axis, allowing radiation coming from recombination to arise only in a thin sheet close to the edge of the boundary layer. Additional effects could arise from transverse shock waves sent into the external medium as the jet material expands transversely to its main flow direction (Komissarov 1994). At the beginning of the flaring jet region, shock-induced pressure and density of the external gas can be expected to be highest. Coupled with photo-ionization from the centre of the galaxy, this could cause reduced $[\text{OIII}]\text{-}5007\text{\AA}$ emission compared to the emission in the region of lower compression further downstream.

The model parameters (Table 1) indicate that the in-

clination of the axes of the out-flows with respect to the plane of the sky is very small ($\sim 10^\circ$). Hill et al. (1988) suggested that the emission-line spiral structure is due to the residual of the interaction between the jet and the interstellar medium, which then is dragged away from the jet path by rotation. Since the spiral features are observed out to the visible edge of the (disk) galaxy, the jet must have propagated close to the plane of the galaxy in order to encounter sufficiently dense material to interact with up to the edge of the galaxy. In this case the distance measures along the jet line are largely unaffected by projection effects. If IRAS 04210+0400 is a disk galaxy, the almost circular appearance of the continuum image (Paper I) suggests that it is oriented close to face-on. Unfortunately the classification of the galaxy is still unclear. In order to settle this question detailed optical and radio observations will be necessary to separate the effect of the emission-line spiral structure from the star light and the paths of the jets. The spiral structure and the implications from a model invoking a jet interacting with the external medium will be studied in a separate paper (Steffen et al. 1996b).

5 CONCLUSIONS

We discussed a simple geometric model of an opening out-flow which reproduces the structure found in the long-slit emission-line spectrum of the hot-spot regions in IRAS 0421+0400. The predicted optical image structure of

these regions is confirmed by deep [O III] line-imaging. The model parameters indicate that the axes of the out-flows lay very close to the plane of the sky, suggesting that the projected distances along their line are largely unaffected by projection. We proposed that a jet crossing a shocked boundary between the interstellar and intergalactic medium could produce such an out-flow in a mixing layer between the jet material and the intergalactic environment. If this model is correct, then IRAS 0421+0400 provides a unique object allowing us to study this phenomenon at optical wavelengths. To date, this has not been possible for the Wide Angle Tail Radio Sources, for which this mechanism has been proposed previously. A more detailed study of this, so far unique source, with as high spatial and spectroscopic resolution and sensitivity is therefore highly desirable.

ACKNOWLEDGEMENTS

AJH and WS acknowledge the receipt of a PPARC studentship and a PPARC research associateship respectively. We thank R.J.R. Williams and A.C. Raga for useful discussions.

REFERENCES

- Beichman C., Wynn-Williams C.G., Lonsdale C.J., Persson S.E., Heasley J.N., Miley G.K., Soifer B.T., Neugebauer G., Becklin E.E., Houck J.R., 1985, *ApJ*, 293, 148
- Cantó J. & Raga A.C., 1991, *ApJ*, 372, 646
- Capetti A., Axon D.J., Macchetto F., Sparks W., Boksenberg A., 1996, *IAU-Symposium 175 on Extragalactic Radio Sources*, Kluwer Academic Publishers, Dordrecht, in press
- Goldstein H., *Classical Mechanics*, 2nd edition, Addison-Wesley Publishing, Inc., 146 f
- Hill G.J., Wynn-Williams C.G., Becklin E.E., MacKenty J.W., 1988, *ApJ*, 335, 93
- Holloway A., Steffen W., Pedlar A., Axon D.J., Dyson J.E. & Meaburn J., 1996 (Paper I), *MNRAS*, 279, 171
- Komissarov S.S., 1994, *MNRAS*, 266, 649
- Loken C., Roettiger K., Burns J.O., Norman, M.L., 1995, *ApJ*, 445, 80
- Norman M.L., Burns J.O., Sulkanen M.E., 1988, *Nature*, 335, 146
- O'Donoghue A.A., Eilek J.A., Owen F.N., 1993, *ApJ*, 408, 428
- Owen F.N., O'Dea C.P., Keel W.C., 1990, *ApJ*, 352, 44
- Soifer B.T., Neugebauer G., Rowan-Robinson M., et al., 1984, *ApJ*, 278, L71
- Steffen W., Holloway A.J., Pedlar A., Axon D.J., 1996a, *IAU-Symposium 175 on Extragalactic Radio Sources*, Kluwer Academic Publishers, Dordrecht, in press
- Steffen W., Holloway A.J., Pedlar A., 1996b, *MNRAS*, in press

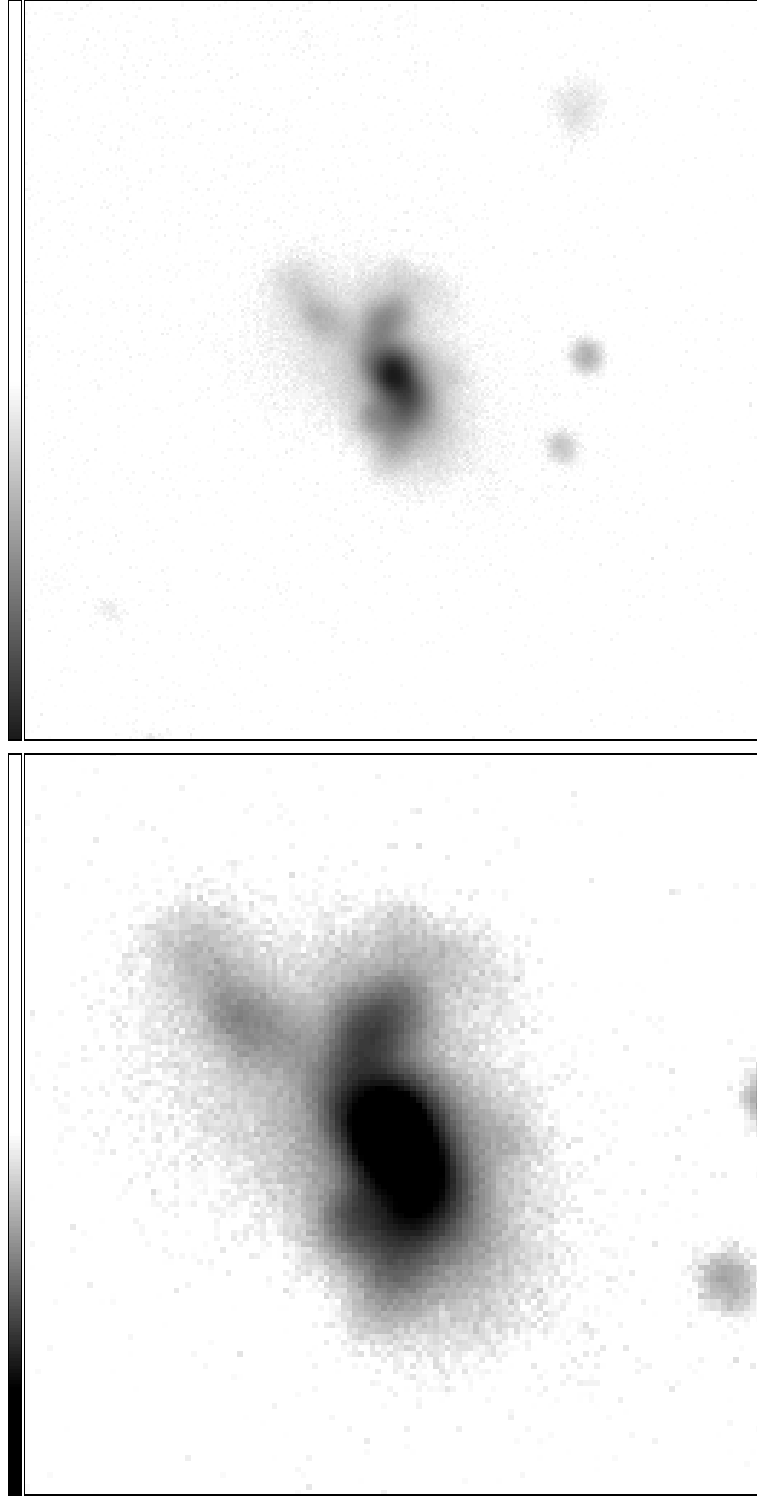


Figure 9. A grey-scale representation of a deep $[\text{OIII}]\text{-}5007\text{\AA}$ image taken at the Anglo-Australian Telescope is shown in the top panel (a), which emphasizes low brightness features at the edge of IRAS 04210+0400. Note the faint, but clearly detected, bifurcation at the northern edge (north is towards the top). It also shows the near environment which is composed by a small companion galaxy at $\sim 11''$ and other barely resolved objects. Several unresolved foreground stars are also seen. The bottom panel (b) shows IRAS 04210+0400 only with its companion. The grey-scale was chosen such that the emission-line spiral structure is emphasized.